Contents lists available at ScienceDirect

Chemical Engineering & Processing: Process Intensification

journal homepage: http://ees.elsevier.com

Bluff-body effect on thermal and NO_x emission characteristics in a micro-planar combustor fueled with premixed ammonia-oxygen

Tao Cai [a], Dan Zhao [a,*], E. Jiaqiang [b]

[a] Department of Mechanical Engineering, College of Engineering, University of Canterbury, Private Bag 4800, Christchurch 8140, New Zealand
[b] College of Mechanical and Vehicle Engineering, Hunan University, Changsha 410082, China

ARTICLE INFO

Keywords
NO*x* emission
Ammonia
Bluff-body
Micro-combustion
Thermal performance
Dimensionless pressure loss

ABSTRACT

In this work, we examine the bluff body effect on thermal and NO_x emission performance in a micro-planar combustor fueled with premixed ammonia/oxygen using three-dimensional numerical simulations. For this, a three-dimensional model is developed with a detailed chemical kinetic mechanism. The effects of 1) the presence/absence of the bluff-body, 2) its dimensionless height h and 3) its dimensionless axial location l are examined. It is found that the implementation of a bluff-body can significantly affects the thermal and NO emission characteristics. Up to 39.1 % reduction of NO formation and 41.6 K increase in the outer wall temperature (OWT) can be achieved as the bluff-body is optimized, when compared to the case in the absence of the bluff-body. Furthermore, increasing h leads to OWT being increased, but it can suppress the NO generation in some cases. In addition, increasing l is shown to be involved with a high OWT and a low NO concentration, mainly due to the variation in the flow field and thus heat transfer characteristics. Finally, the dimensionless pressure loss is strongly affected by the NH_3 flow rate, and the dimensionless parameters h and l. This work reveals that implementing a proper designed bluff-body is an effective way to enhance thermal performance and reduce NO_x emission.

1. Introduction

Chemical combustion has been playing a critical role in power generation and propulsion industry sectors. It is an important energy conversion process in many power generation or propulsion systems, such as internal combustion engines and gas turbine engines. With fossil fuels involved combustion being one of the main contributor to the climate change, it is of great desire to search for potential and greenhouse gas-free alternatives [1]. Among the potential candidates, hydrogen is one of the most advocated fuels, as there is no greenhouse gases emission such as CO_2 and the only combustion product is water. However, due to the high mass diffusivity, it is difficult to store and transport hydrogen, thus hindering its usage as a suitable alternative [2,3]. By contrast, ammonia with a high hydrogen density (17.7 wt%) is gaining much attention worldwide, as NH_3 combustion does not lead to the emissions of CO_2 and carbon-involved soot. Meanwhile, it is also advantageous in terms of storage and transportation because of the low laminar flame speed [4,5]. In addition, ammonia can be produced in various ways in an eco-friendly way [6,7]. These features make it more competitive compared to hydrogen and hydrocarbon fuels in energy conversion devices.

Ammonia-based combustion for industrial power generation systems is not a new ideas. The first application fueled with ammonia was produced in Belgium in 1942 [8]. Over the past few decades, gas turbine engines that burn ammonia has been of particular interest and intensive research has been conducted, as it is carbon-free fuel and energy carrier. Verkamp et al. [9] experimentally examined the minimum ignition energy and the quenching distance of remixed ammonia/air in gas turbine combustor. In order to gain a better understanding of ammonia-fueled combustion, Hayakawa et al. [10] recently performed an experimental study on the ammonia combustion in a swirl combustor. It was shown that stable flame could be realized, even if there were no additives. Three-dimensional large-eddy simulations (LES) were performed to shed light on the combustion characteristics of ammonia swirl flames [11]. Somarathne et al. [12] conducted numerical investigation on the emission characteristics of ammonia/air turbulent flames in a swirl combustor under high pressure conditions. The local temperature was shown to play an important role in affecting the local NO generation rate. Furthermore, there was a minimum NO emission with

* Corresponding author.
E-mail address: dan.zhao@canterbury.ac.nz (D. Zhao)

https://doi.org/10.1016/j.cep.2020.107979
Received 10 March 2020; Received in revised form 3 May 2020; Accepted 18 May 2020
Available online xxx

the global equivalence ratio of 1.1, whatever the wall thermal condition was set.

In order to improve the thermal and emission characteristics of ammonia-fueled gas turbine engines, a number of approaches have been proposed through experimental measurements and numerical studies. Note that ammonia has a relatively narrow flammability limits and a large ignition energy in comparison with hydrogen and hydrocarbon fuels [13,14]. Co-combustion is expected to positively affect the ammonia combustion when blending with the hydrogen and/or hydrocarbon fuels. The most commonly used additives are hydrogen and methane [15–20]. Valera-Medina et al. [15] conducted premilinary studies on the emission performance of NH_3-H_2. It was found that there was a narrow operating limit with the possibility of flame flashback due to the H_2's high diffusivity. The NO_x emission was shown to increase because of the excess OH and O radicals. Further numerical and experimental investigations on the flame stability and emissions characteristics of ammonia-methane swirling flames were conducted [17]. It was demonstrated that stratified injection with a low swirl intensity could be regarded as the most effective means when using binary fuel. In addition, the initial conditions such as pressure and temperature were proven to play a key role in the NO_x generation [12,21,22]. Somarathne et al. [21] demonstrated that NO formation was greatly sensitive to the pressure. A higher pressure was shown to be involved with a low NO concentration using LES.

Foregoing studies show that ammonia combustion has been of great interest in many industrial applications, especially for gas turbine engines. However, could ammonia combustion be applied in small-size combustion systems? Such small-combustor with hydrogen or hydrocarbon fueled is a critical component in micro-power generation [23–26]. There have been few attempts on ammonia-fueled micro-power systems [27–30]. Nakamura et al. [27,28] developed a chemical kinetic model to examine the presence of a weak flame within a temperature-controlled micro-combustor. They confirmed that weak flames could be utilized to validate chemical kinetic mechanism for ammonia-fueled micro-combustion. In addition, Okafor et al. [29] demonstrated the possibility of a stable power generation in an ammonia-fueled micro gas turbine with a high combustion efficiency. The micro power generation system is more attractive in comparison with conventional lithium batteries [31,32] due to a higher energy density, and a longer operating lifespan. The previous studies reveal that ammonia has a greater potential to be used as a renewable and sustainable fuel. However, to the best knowledge of the present authors, there are few reports on the NO_x emissions of burning ammonia in micro-planar combustors. This type of micro-combustors is widely integrated in micro-thermophotovoltaic systems [33,34]. This partially motivates the present work.

In this work, a bluff-body is designed and implemented in a micro-planar combustor to gain insight on thermal performance and NO_x emission of ammonia combustion. For this, 3D simulations are performed to shed light on how the bluff-body affects the inner flow field and thus outer wall temperature distribution as well as NO formation. In Section 2, the geometry and dimensions of the bluff-body involved combustor and the corresponding computational model are described. Mesh independence study and chemical reaction kinetic mechanism validation are then carried out. In Section 3, the effects of the bluff-body dimensionless height h as well as its dimensionless axial location l are examined and discussed. Comparison is made with the case in the absence of the bluff-body. Finally, key findings are summarized in Section 4. An optimum design of the bluff-body involved micro-combustor is obtained from the perspectives of thermal performance and NO emissions.

2. Description of computational method

2.1. Geometric model

A micro-planar combustor in the presence of a rectangular-shaped bluff-body is numerically modelled as shown in Fig. 1. This is to evaluate the effect of the bluff body on the thermal and NOx emission characteristics of the combustor. The total length, width and height of the combustor are set to $L = 20$ mm, $W = 11$ mm and $H = 3$ mm, respectively. The wall thickness is $t = 0.5$ mm. Therefore, the combustion channel width and height are 10 mm and 2 mm. The bluff-body is implemented at the axial location L_1 away from the combustor inlet (with reference to the flow direction). The length of the bluff-body is $L_2 = 1$ mm, while the width remains same as the channel width. As for the height and location of the bluff-body, they are varied from cases to cases for comparison. Note that the dimensionless height h is defined as the ratio of bluff-body height H_1 to the combustion flow channel height. The dimensionless bluff-body location l denotes the ratio of the distance of bluff-body away from the combustor inlet to the combustion channel length. The whole combustor is assumed to be made from the steel.

2.2. Computational model

In the present work, ANSYS (Fluent 18.1) is adopted to systematically solve the governing equations related to the 3D model of flow-combustion-thermodynamics-heat transfer coupling, which include the mass continuity, momentum, energy and species governing equations. The detailed chemistry mechanism for ammonia/oxygen combustion involves 22 elementary species and 67 reversible reactions [35]. The pressure-velocity coupling is solved using SIMPLE algorithm, whilst the

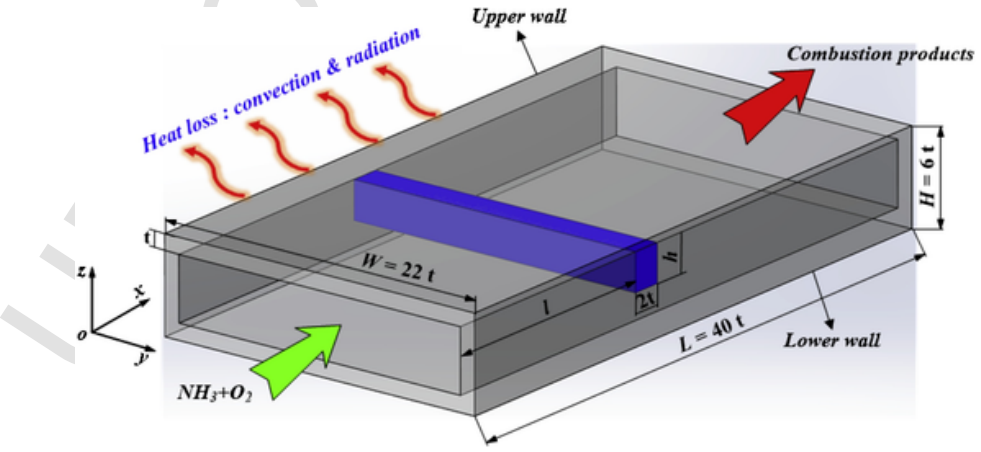

Fig. 1. Geometric dimensions of the simplified micro-planar combustor with bluff-body.

governing equations and species are discretized by the second-order upwind scheme. The convergence criterions for all residuals are set less than 10^{-6}.

The inlet boundary condition is set to velocity inlet in all the tested cases in this work. The maximum flow velocity is 1.75 m/s, with a corresponding Reynolds number of 367. Therefore, the laminar flow model is assumed to occur in the combustor as suggested by Ronney et al. [36]. The chemical reaction is calculated by finite rate model. Regarding each species, the specific heat is obtained based on a piecewise polynomial fit of temperature, while the thermal conductivity and viscosity are computed by using the kinetic-theory [37]. When it comes to fuel-oxy mixture, the specific heat is solved based on the mixing-law, whilst the ideal-gas-mixing law is used for both the thermal conductivity and viscosity [37]. In addition, the pressure diffusion is neglected due to a small magnitude [38,39]. In order to improve the accuracy of computation results, the gas radiation between the inner walls and the mixture is considered [40]. For mass and energy diffusion, Soret effect is considered since it plays an important role in NO production rate, while Dufour effect has a minimal effect [41]. The NO_x model is ignored since it is not compatible with the premixed combustion [37].

For the inlet of the micro-combustor, a uniform velocity profile with an initial temperate of 300 K is assumed and the gauge pressure is zero. When it comes to the combustor outlet, pressure-outlet boundary condition is considered. As for gas-solid interfaces, zero diffusive flux species and no slip boundary condition are assumed. Mixed thermal conditions including radiation and convection heat transfer are chosen for all external walls [42,43]. Thus, the heat loss can be calculated by the Eq. (1):

$$q = h\left(T_W - T_\infty\right) + \varepsilon\sigma_b\left(T_W^4 - T_\infty^4\right) \quad (1)$$

where h represents natural convective heat transfer coefficient (20 $W/m\cdot K$ from Wan et al. [44]); T_W is the temperature at the external wall surface; T_∞ denotes the ambient temperature (300 K); ε stands for the solid emissivity (0.85); σ_b is the Stephan-Boltzmann constant ($5.67\times10^{-8} W/m^2\cdot K^4$).

2.3. Grid independence and mechanism comparison studies

The mesh independence analysis is of great importance in balancing the accuracy of calculated results and computational expense. For this, three different number meshes are generated by using Gambit 2.4.6, i.e., the fine (elements: 352,000), medium (elements: 168,000) and coarse mesh (elements: 89,000). Note that the ratio of fuel to oxidizer is set to 1.0 for all computational cases in this work. Fig. 2 illustrates the calculated centerline temperature profiles on the cross section in the streamwise direction with three different number of grid cells, as the NH_3 volumetric flow rate is set to 400 mL/min. It can be seen that centerline temperature profiles are almost the same in the shape, whatever the cell number is set to. However, it should be pointing out that there is significant difference in the axial location of the peak temperature between the coarse and medium grid densities. By contrary, this discrepancy is negligible among the medium and fine meshes. This indicates that the medium grid is able to satisfy the computational requirements and be chosen for all simulations in the following work.

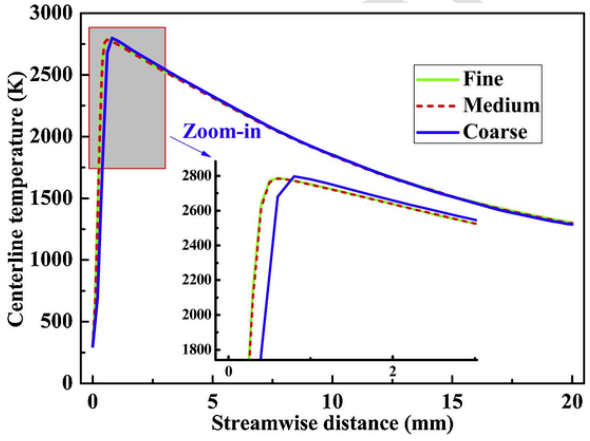

Fig. 2. Comparison of the axial temperature profiles on the cross-section from the combustor inlet, as the grid cells are set to 3 different values.

Since little attention is paid to ammonia combustion in a small-size combustor, the NH_3 chemical reaction mechanism in micro-combustor is not well-investigated. Fortunately, the detailed kinetic mechanism of ammonia-fueled combustion in a micro-flow reactor was reported and proved to be applicable [27]. Therefore the results obtained from the current mechanism [35] will be compared to those from the one proposed by Nakamura et al. [27]. Fig. 3 shows the variation of the outer wall temperature (OWT) and the NO concentrations at the combustor outlet using two different chemical reaction mechanisms under various NH_3 volumetric flow rates. Herein, the OWT denotes the mean temperature of the top and bottom combustor wall. Considering the fact that the computed concentrations of nitrogen dioxide (NO_2) and nitrous oxide (N_2O) during combustion are negligible in comparison with NO. Herein, NO generation can be treated as an indicator of the NO_x emissions. This assumption was also confirmed in the previous works [43,44] both numerically and experimentally. It can be seen from the Fig. 3 that there is a good agreement in the OWT calculated from the two reaction mechanisms, no matter what the fuel flow rate is set. It is found that the maximal relative error is only 1.3 % with the fuel flow rate being set to 400 mL/min. Furthermore, the NO concentrations also show the similar trend. These indicate that the present chemical kinetic mechanism is able to reflect and reveal the combustion characteristics of a premixed ammonia/oxygen under micro-scale conditions.

2.4. Validation of the numerical model

To verify and demonstrate the accuracy of the computational model, the computed temperature contour on the combustor outer wall is explored and compared with the experimental data [45]. This is illustrated in Fig. 4, as the inlet velocity of the mixture is set to 0.6 m/s and the fuel-oxidizer ratio is 1.0. It can be seen that the computed temperature distribution from the methane-air fueled combustor matches well with the experimental result (see Fig. 4(a) and (b)). However, there are some differences in the location of the peak temperature between the methane and ammonia combustion (see Fig. 4(b) and (c)).

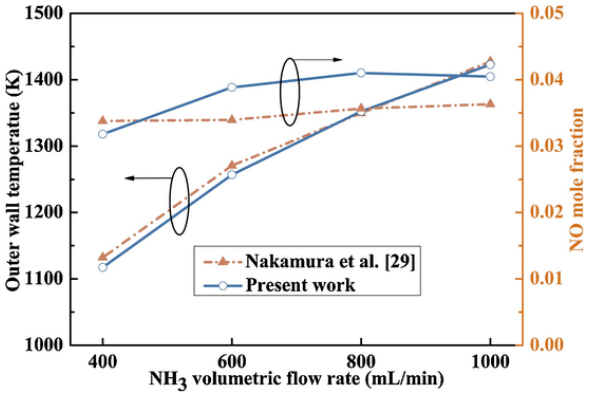

Fig. 3. Comparison of the computed outer wall temperature and NO mole fraction at the combustor outlet using two different kinetic mechanisms under various fuel volumetric flow rates. One is taken from Ref. [27], and the other mechanism is discussed by Drake and Blint [35].

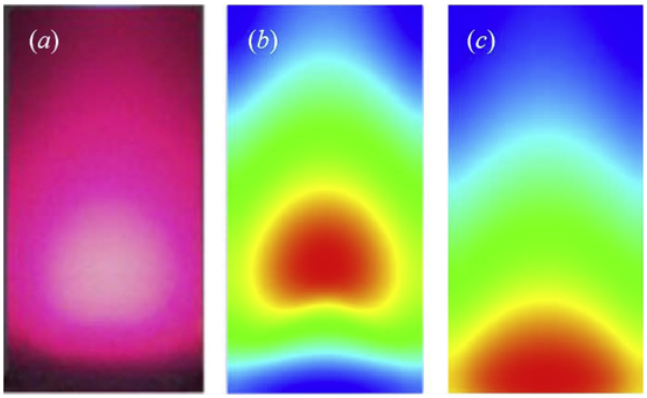

Fig. 4. Comparison of the calculated temperature contours on the outer wall: (*a*) experimental data of a methane-air flame [45]; (*b*) numerical data of a methane-air flame; (c) numerical data of an ammonia-oxygen flame.

In other words, the ammonia flame is much closer to the combustor than the methane flame.

In addition, we further investigate the centerline temperature profiles on the combustor outer wall along the axial direction, as the inlet velocity of mixture is set to 2 different values. This is shown in Fig. 5. It is clear that the calculated temperature profiles from the methane-burnt combustor are consistent with those through experiment in terms of the shape as well as the location of the peak temperature. The maximal relative error with a value of 5.1 % occurs at 3 mm away from the combustor inlet, as the inlet velocity is set to 0.6 m/s, corresponding to the methane volumetric flow rate of 55 mL/min. Furthermore, it is worth noting that the temperature profile for ammonia-oxygen combustion is quite different from those in methane/air-fueled combustor, whatever the inlet velocity is set to. This is most likely due to the variation in the oxidizer. Note that the flame burning velocity for the fuel/oxygen flames is dramatically higher than that of for the fuel/air flames [41]. Comparing Fig. 4 and 5 reveals that the present numerical model is reasonably accurate. It can be utilized in simulating micro-combustion processes.

3. Results and discussion

3.1. Performances comparison of micro-combustors with and without a bluff-body

In order to evaluate the effect of the bluff-body on combustion performance, comparison is first made in terms of outer wall temperature (OWT) and NO generation. Fig. 6 shows the variation of the outer wall

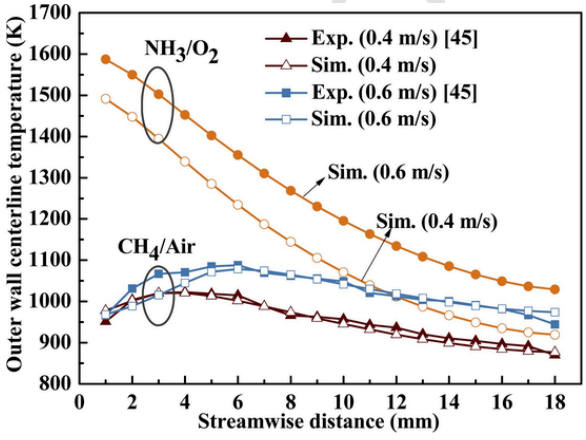

Fig. 5. Comparison of the centerline temperature profiles between the experiment [45] and simulation results.

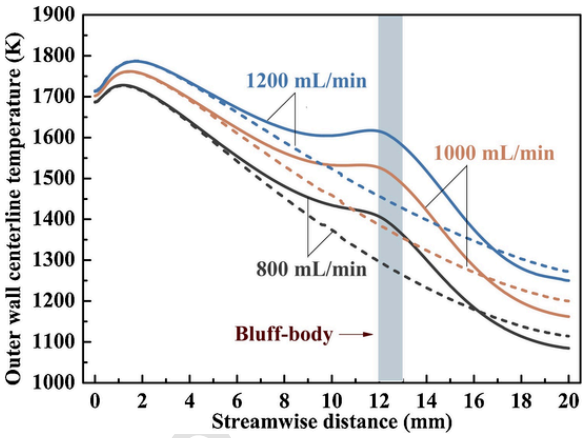

Fig. 6. Comparison of the centerline temperature profiles along the combustor outer wall with (solid lines) and without (dashed lines) bluff-body implemented, as the NH_3 volumetric flow rates is set to 3 different values.

temperature profiles on the bottom wall along the streamwise direction without and with a bluff-body (h = 4/5, l = 3/5), as the NH_3 volumetric flow rate is set to 3 different values. It is clear that the temperature profiles have the similar tendency, i.e., it increases first, and then decreases in the streamwise direction as the chemical reaction takes place. In addition, it can be seen that there are negligible differences in the temperatures in the presence or absence of the bluff-body close to the combustor inlet, no matter what fuel flow rate is set to. By contrast, in the vicinity of the bluff-body, the wall temperatures is significantly higher compared to that in the absence of the bluff body. However, near the combustor outlet, the temperatures tend to be slightly lower in such a bluff-body combustor. Accordingly, it can be concluded that the OWT with a bluff-body inserted should be much higher than those in the absence of the bluff-body, implying that the bluff-body has an influence on affecting the heat transfer characteristics to some extent.

The bluff-body effect on NO formation is also examined and discussed, as the NH_3 flow rate is set to 3 different values. This is illustrated in Fig. 7. It can be seen that at a relatively low fuel flow rate (≤ 1000 mL/min), there are slight differences in the NO generation at the combustor outlet whether the bluff-body is implemented or not. A considerable discrepancy, however, can be observed, as the fuel flow rate reaches 1200 mL/min. Up to 8.4 % reduction in NO concentrations in the presence of such bluff-body can be observed in comparison with that in the absence of the bluff-body. This indicates that the bluff-body may play a negligible role in the NO formation at a low fuel flow rate.

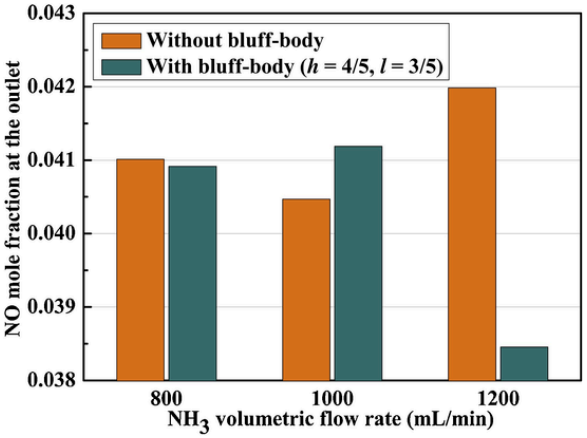

Fig. 7. Comparison of the NO mole fraction from the combustor with and without bluff-body implemented at various NH_3 volumetric flow rates.

To further understand the mechanism contributing to the OWT variation as well as NO formation, the temperature profiles along the axial direction are determined, when the fuel flow rate is set to 1200 mL/min. This is shown in Fig. 8. It is clear that the temperature field distribution in the presence of the bluff-body is quite different from that without the bluff-body, especially in the vicinity of the bluff-body, the implying that the bluff-body plays a critical role in affecting the flow field. A close examination of Fig. 8 shows that compared to the case in the absence of the bluff-body, there is a region where the flame temperatures downstream of the bluff-body along the streamwise direction are dramatically lower. The decreased flame temperature is effective in reducing the NO generation rate. Furthermore, it is worth noting that the flame temperature near the bottom wall is quite high when compared to the case without a bluff-body implemented, which helps enhance the heat transfer between the flowing gases and the bottom wall. The above results suggest that the high flame temperature near the bottom wall and the region with a low flame temperature formed downstream of the bluff-body are responsible for the increased outer wall temperature and reduced NO production respectively.

3.2. Effect of bluff-body dimensionless height h

Considering the variations in the thermal and emission performances in the presence of the bluff-body, it would be interesting to know the influence of varying its geometry structure. Let us first consider the effect of the bluff-body height. To make our analysis more generalized, dimensionless height h is used. Fig. 9 shows the variation of the outer wall temperature (OWT) of the bluff-body involved micro-combustor with the height h, as $l = 4/5$ and the NH_3 volumetric flow rate is set to different values. Considering the temperature difference between the top and bottom combustor walls and to make our analysis more generalized, the average temperatures of both the top and bottom walls is used and denoted by OWT. It can be seen that increasing the fuel volumetric flow rate gives rise to an increase of OWT, but the temperature increment becomes smaller at the same increment of the flow rate, irrespective of h. This is due to the fact that an increase in the flow rate can cause the reduced residence time of the mixture in the channel and thus the weakened heat transfer. Furthermore, it is worth noting that for a fixed NH_3 flow rate, OWT is found to increase with increased h. The enhancement performance is more obvious at a higher fuel flow rate. For instance, the temperature difference between $h = 1/5$ and $4/5$ at a fuel flow rate of 600 mL/min is estimated to be 9 K. In contrast, the temperature variation is increased to be approximately 23.5 K, as the fuel flow rate is increased to 1200 mL/min. This reveals that increasing the bluff-body height has a greater potential on improving the thermal performance.

The presence of a bluff-body is able to change the flow characteristics and thus the pressure variation. The large pressure variation is normally associated with the high power cost of fuel pumped, which is undesirable in power generation systems. Thus it is meaningful to examine the pressure loss. The dimensionless pressure loss is defined as:

$$P_{loss} = \frac{P_{in} - P_{out}}{P_{amb}} \tag{2}$$

where P_{loss} denotes the dimensionless pressure loss, P_{in} and P_{out} stand for the pressure on the channel inlet and outlet respectively, and P_{amb} represents the ambient pressure.

Fig. 10 illustrates the dimensionless pressure loss P_{loss} as a function of the fuel flow rate at various h. It can be seen that for a given h, increasing the fuel flow rate leads to P_{loss} being further increased. This is consistent with the previous reports [46,47]. Meanwhile, it is worth noting that P_{loss} increases with different slopes as a function of the NH_3 flow rate. The change in slope is associated with the acceleration experienced by the fluid elements. It can be also observed that at a low value of bluff-body height ($h \leq 2/5$), there is a little difference in the dimensionless pressure loss, whatever the fuel flow rate is set to. In contrast, a considerable increase in P_{loss} can occur when further increasing h from 2/5 to 3/5. Nevertheless, when h is set to 4/5, P_{loss} is shown to be sharply increased. This indicates that in addition to increasing the fuel flow rate, increasing h can also lead to a greater pressure fluctuation. This is because a large h is more effective in changing the flow field distribution.

Since the outer wall temperature is affected by h to some extent, it is interesting to know its impact on the NO generation. Fig. 11 illustrates the NO mole fraction at the combustor outlet varied with h, as the NH_3 volumetric flow rate is set to 4 different values. It can be seen that the NO concentration presents a non-monotonic tendency as a function of the fuel flow rate, i.e., it is increased first and then decreased with increasing NH_3 flow rate, regardless of h. The explanation for this phenomenon could be attributed to two aspects. First, the increase in the NH_3 flow rate means more N atoms in the mixture. This in turn leads to more NO being generated due to a higher temperature. On the other hand, the residence time of combustion products in the channel is reduced with increasing the NH_3 flow rate, which helps to dampen the NO formation. The two effects play a competing role in NO_x emissions. Furthermore, increasing h can result in the NO concentration being increased first and then decreased, whatever the fuel flow rate is set to. In general, a bluff-body with $h = 4/5$ is more likely to be involved with a less NO production, especially at a high fuel flow rate with a value of 1200 mL/min. These observations confirm that the NH_3 flow rate and the dimensionless height h play a critical role in determining the NO_x formation behavior.

To provide greater insight into how the bluff-body height impacts the combustion characteristics, we further explore the flow field characteristics in the presence of the bluff-body. Fig. 12 illustrates the velocity field contours overlapped with streamlines at various h, as the NH_3 volumetric flow rate is set to 1200 mL/min. It is clear that there is a recirculation zone formed around the bluff-body, no matter what h is

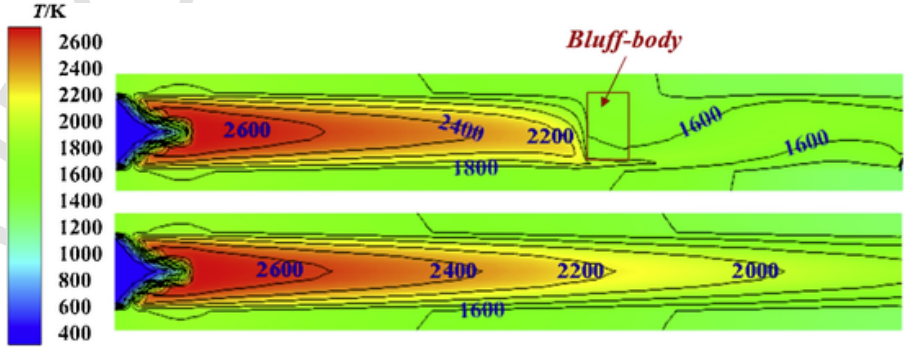

Fig. 8. Comparison of the temperature contours overlapped with streamlines in combustors with and without bluff-body applied.

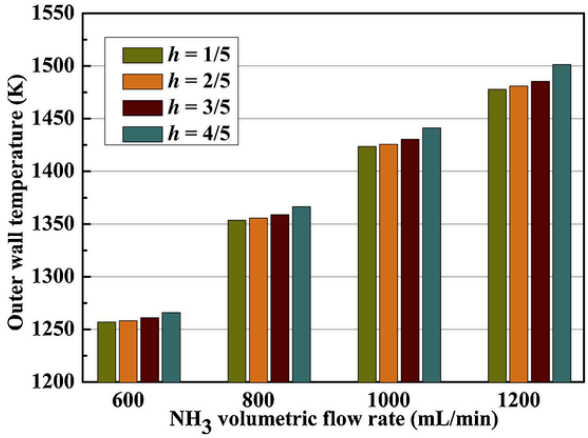

Fig. 9. Variation of outer wall temperature with NH_3 volumetric flow rate, as the dimensionless bluff-body height h is set to 4 different values.

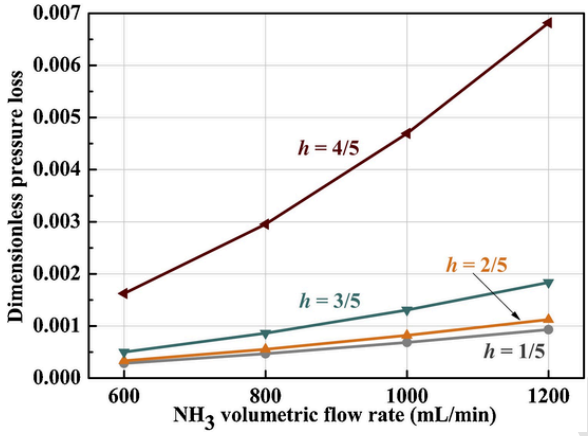

Fig. 10. Variations of dimensionless pressure loss as a function of NH_3 flow rate, as the dimensionless bluff-body height h is set to 4 different values.

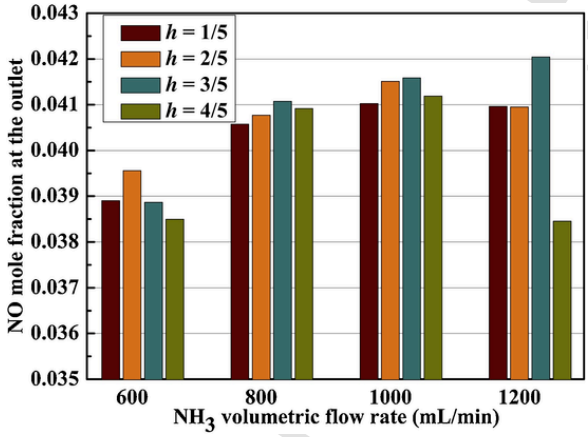

Fig. 11. NO mole fraction as a function of NH_3 volumetric flow rate varied with dimensionless height h.

set to. However, the size of the recirculation zone varies significantly. The combustor with a greater h is shown to be associated with a large recirculation zone and a higher flame velocity near the bottom wall/surface, which can lead to the large pressure loss. These results are consistent with the data shown in Fig. 10. In addition, it is worth pointing out that as h is increased, the gases are more likely to flow along the combustor bottom wall and thus enhance the heat transfer with the wall. Comparing Figs. 9–12 reveals that both the OWT, the dimensionless pressure loss as well as NO formation are highly sensitive to the bluff-body height due to the change in the flow field and thus the heat transfer.

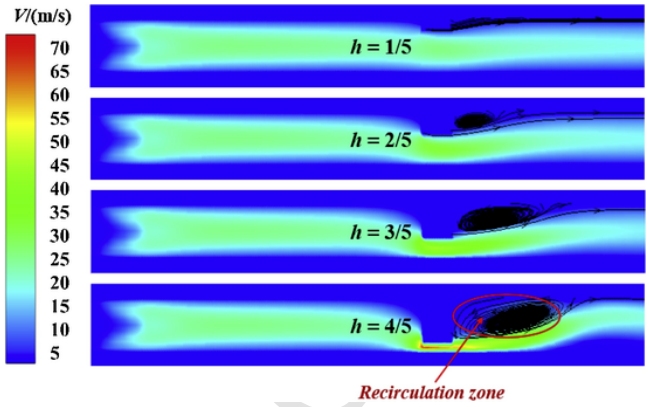

Fig. 12. Velocity field contours overlapped with streamlines with NH_3 volumetric flow rate being set to 1200 mL/min, as h is set to 4 different values.

3.3. Effect of bluff-body dimensionless location l

It would be interesting to know the changes of the thermal and NO emission behaviors, as the bluff-body dimensionless axial location l is varied. This is achieved by varying l from 1/5 to 4/5 at an interval of 1/5, as the height remains the same, i.e., $h = 4/5$. Fig. 13 shows the variation of the outer wall temperature (OWT) with NH_3 volumetric flow rate, as l is set to 4 different values. It can be seen that OWT varies significantly with varied l. In general, a higher l is found to be associated with a high OWT. Moreover, it can be noted that for a given NH_3 flow rate, a noticeable increase in OWT can be observed, as $l = 1/5$ is increased to 2/5. However, the increased increment gradually becomes smaller with further increasing l. This suggests that the effectiveness of the bluff-body in improving OWT is highly dependent on its axial location.

Fig. 14 illustrates the dimensionless pressure loss P_{loss} variation with NH_3 flow rate, as the dimensionless axial location l is set to different values. It is apparent that a higher fuel flow rate is associated with a greater pressure fluctuation, whatever l is set to. Another feature shown in Fig. 14 is that P_{loss} varies at different slopes for a given l. When the bluff-body is located at 1/5, P_{loss} is minimal. However, there is a significant increase of P_{loss}, as the bluff-body is placed at 2/5. The significant increase of the P_{loss} can be due to the fact that the bluff-body is placed at a pressure node location. At such location, a maximal

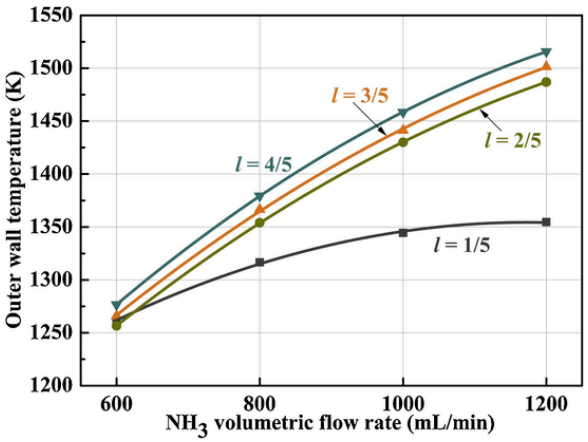

Fig. 13. Comparison of the outer wall temperature variation with NH_3 volumetric flow rate, as l is set to 4 different values.

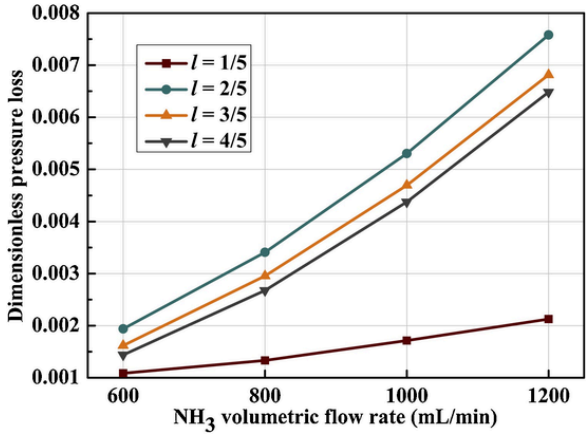

Fig. 14. Variations of dimensionless pressure loss as a function of fuel flow rate, as the dimensionless bluff-body location l is set to 4 different values.

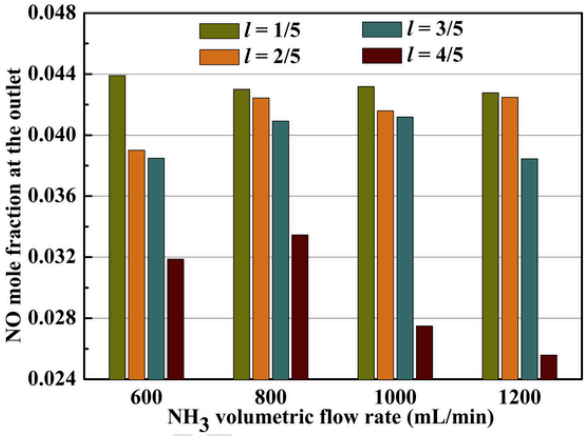

Fig. 16. Comparison of NO mole fraction as a function of NH_3 volumetric flow rate varied with l.

pressure fluctuation is expected. However, further increasing h to 3/5 and 4/5 gives rise to a decreased pressure drop. This reveals that the pressure loss is not a linear function of dimensionless axial location l.

To gain a better understanding of how the dimensionless l affects thermal and pressure loss behaviors, we further examine the flow field distribution inside the combustor. Fig. 15 shows the velocity field contours overlapped with streamline varied with l, as the NH_3 volumetric flow rate is set to 1200 mL/min. It is clear that there are recirculation zones formed downstream of the bluff-body. However, the size of these regions is quite different, as the bluff-body is placed at different locations. In addition, it should be pointing out that the flame velocity in the channel is maximized at l = 2/5, followed by l = 3/5 and 4/5, and then l = 1/5. This qualitatively explains the order of the dimensionless pressure loss variation illustrated in Fig. 14. Although the flame velocity peaks at l = 2/5, it is not necessarily involved with a highest OWT shown in Fig. 13. This can be attributed to the fact that when the bluff-body is placed far away from the combustor outlet ($l \leq 3/5$), the stream after the bluff-body is not able to flow along the combustor bottom wall, thereby leading to the poor heat transfer characteristics.

In view of the discrepancy in OWT by varying l, it is meaningful to know its effect on NO formation, which strongly depends on the flame temperature. Fig. 16 shows the variation of the NO mole fraction at the combustor outlet with NH_3 volumetric flow rate, as the l is set to 4 different values. It can be seen that for a given l, NO concentration is changed as the fuel flow rate is varied. For instance, when l = 1/5, NO emission is less affected by the fuel flow rate in comparison with that when l is set to other value. However, when $l \geq$ 2/5, there are some

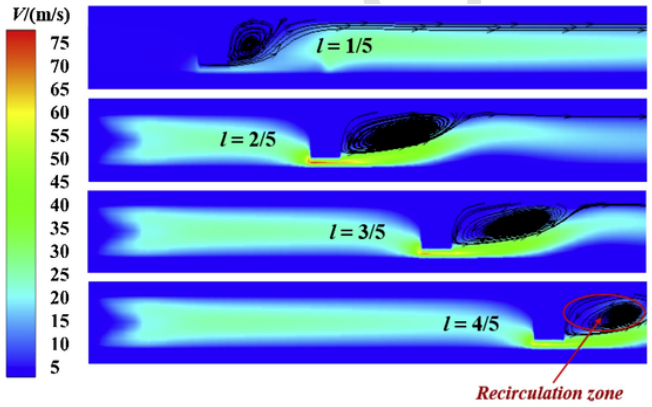

Fig. 15. Velocity field contours overlapped with streamlines at various NH_3 volumetric flow rates and the dimensionless bluff-body locations l.

certain differences. Another feature shown in Fig. 16 is that the NO production varies significantly with varied l, no matter what the fuel flow rate is considered. Increasing l is shown to remarkably reduce the NO generation rate. The NO mole fraction with l = 1/5 is almost twice as large as that of l = 4/5. These results indicate that the NO generation rate is strongly related to l and the NH_3 flow rate. In general, these results reveal that choosing a proper l can improve the thermal performance and reduce NO_x emissions. This is most likely due to the enhanced heat transfer between the flowing gases and the combustor bottom wall as well as the region with a lower flame temperature downstream of the bluff-body respectively. By comparing Figs. 6,7, 13 and 15, it is found that up to 39.1 % reduction in NO formation and 41.6 K increase in OWT can be achieved in the presence of the bluff-body with h = 4/5 and l = 4/5 compared to those without a bluff-body, as the NH_3 flow rate is set to 1200 mL/min.

To shed light on how the bluff-body dimensionless axial location l affects NO_x emission behaviors, we further examine the NO distribution along the axial direction of the combustor. Fig. 17 shows the NO contours varied with l, as the NH_3 volumetric flow rate is set to 1200 mL/min. It is clear that at different l, the NO distribution is different to some extent. That is, when l = 1/5, the NO concentration peaks after the bluff-body. This is because when the bluff-body is placed too close to the combustor inlet, the fuel-oxidizer mixture cannot be ignited as soon as it enters the channel due to the large inlet velocity. However, when l is above 1/5, the bluff-body has little influence on the ignition process and the NO concentration tends to peak near the combustor inlet. Furthermore, a closer examination on Fig. 16 shows that when $l \geq$ 3/5, there are local regions associated with a low NO concentration close to the combustor outlet. This is in accordance with the data presented in Fig. 16 and qualitatively explains the mechanism on the reduced NO emissions with a bluff-body implemented.

4. Conclusions

To enhance thermal performance and reduce NO_x emissions, a bluff-body is implemented in a micro-planar combustor with ammonia and oxygen fueled. For this, a 3D numerical model with detailed chemistry and multicomponent transport is developed. Validation of the reaction mechanism and the numerical model is conducted first. Preliminary studies on the combustion characteristics of such micro-combustor are then carried out by comparing the cases in the presence and absence of the bluff-body. Further investigations on the effects of the bluff-body dimensionless height h as well as its' axial location l are performed to shed light on the optimum configuration of the bluff-body. The main concluding remarks are summarized as:

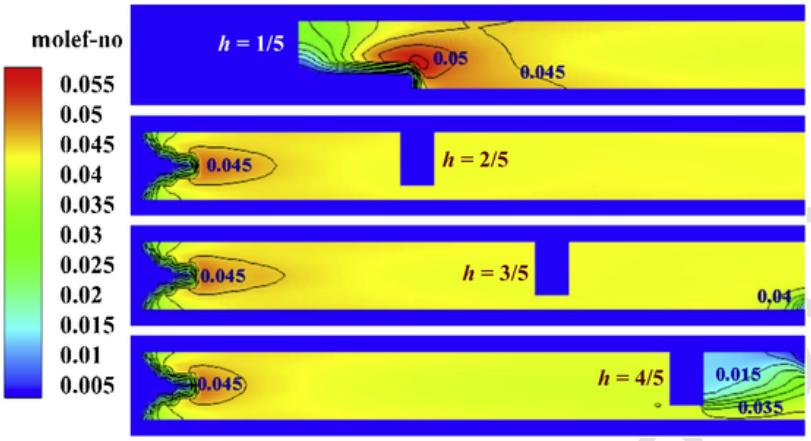

Fig. 17. NO contours on the vertical-section with NH_3 flow rate being set to 1200 mL/min, as l is set to 4 different values.

- When there is a bluff-body, the centerline temperatures of the combustor bottom wall along the streamwise direction are significantly higher than that of in the absence of the bluff-body, mainly due to the change in the flow field. In addition, the implementation of the bluff-body is able to reduce the NO generation rate under some conditions.
- OWT is found to be increased with increasing h, irrespective of the NH_3 flow rate. A large h is associated with a greater recirculation zone with a low flame temperature, which is effective in dampening the NO formation. Meanwhile, the stream at high h is more likely to flow along the combustor bottom wall, leading to the enhanced heat transfer and thus a high OWT. Furthermore, it is found that the dimensionless pressure loss P_{loss} is linearly dependent on h, that is, the higher h, the greater P_{loss} will be.
- The bluff-body location plays a key role both in the thermal and NO generation characteristics. Increasing l is shown to lead to OWT being increased, but the NO generation rate being reduced. This is most likely due to the fact that as l is increased, the heat transfer between the mixture and the combustor bottom wall is much more intensive. Further analysis indicates that when the bluff-body is placed near the combustor outlet, there are some areas with a low NO concentration, due to the low flame temperature. Furthermore, the dimensionless pressure loss tends to be increased first and then decreased with l. This is quite different from that regarding h.
- The optimum dimensions of the bluff-body are identified to be $h = 4/5$ and $l = 4/5$ corresponding to the maximum OWT and minimum NO_x emissions. It is found that up to 39.1 % reduction in NO formation and 41.6 K increase in OWT can be achieved in the optimum designed bluff-body involved micro-combustor in comparison with that in the absence of the bluff-body, as the NH_3 flow rate is set to 1200 mL/min.

In general, the present work confirms that implementing a bluff-body into a micro-planar combustor could be an effective but practical way to minimize NO_x emission and maximize thermal performances.

Authors contributions

T. C conducted numerical simulations and discussed with D. Z and JQ. E. D.Z. edited and revised the manuscript with T. C. D. Z. conceived and initialized the project. All authors contributed to the paper writing.

Declaration of Competing Interest

The authors declare that they have no conflict of interest.

Acknowledgements

We gratefully acknowledge the financial support from the University of Canterbury, New Zealand (grant no. 452STUPDZ) and Singapore National Research Foundation (grant no. NRF2016 NRF-NSFC001-102). Tao Cai would like to thank to College of Engineering, University of Canterbury for providing his PhD studentship.

References

[1] A P Roskilly, M Ahmad Al-Nimr, Sustainable thermal energy management, Energy Convers. Manage. 159 (2018) 396–397.
[2] A Valera-Medina, H Xiao, M Owen-Jones, W I F David, P J Bowen, Ammonia for power, Prog. Energy Combust. Sci. 69 (2018) 63–102.
[3] J Li, H Y Huang, L S Deng, Z H He, Y Osaka, N Kobayashi, Effect of hydrogen addition on combustion and heat release characteristics of ammonia flame, Energy 175 (2019) 604–617.
[4] Q M Liu, X Chen, J X Huang, Y Shen, Y M Zhang, Z W Liu, The characteristics of flame propagation in ammonia/oxygen mixtures, J. Hazard. Mater. 363 (2019) 187–196.
[5] K Takizawa, A Takahashi, K Tokuhashi, S Kondo, A Sekiya, Burning velocity measurements of nitrogen-containing compounds, J. Hazard. Mater. 155 (1–2) (2008) 144–152.
[6] R F Service, Ammonia-a renewable fuel made from sun, air, and water-could power the globe without carbon, Science (2018), http://10.1126/science.aau7489.
[7] C Zamfirescu, I Dincer, Ammonia as a green fuel and hydrogen source for vehicular applications, Fuel Process. Technol. 90 (5) (2009) 729–737.
[8] E Kroch, Ammonia-a fuel for motor buses, J. Ins. Pet. 31 (1945) 213–223.
[9] F J Verkamp, M C Hardin, J R Williams, Ammonia combustion properties and performance in gas-turbine burners, Proc. Combust. Inst. 11 (1967) 985–992.
[10] A Hayakawa, Y Arakawa, R Mimoto, K D Kunkuma, A Somarathne, T Kudo, H Kobayashi, Experimental investigation of stabilization and emission characteristics of ammonia/air premixed flames in a swirl combustor, Int. J. Hydrogen Energy 42 (19) (2017) 14010–14018.
[11] K D K A Somarathne, A Hayakawa, H Kobayashi, Numerical investigation on the combustion characteristics of turbulent premixed ammonia/air flames stabilized by a swirl burner, J. Fluid Sci. Technol. 11 (4) (2016) JFST0026.
[12] K D K A Somarathne, E C Okafor, A Hayakawa, T Kudo, O Kurata, N Iki, H Kobayashi, Emission characteristics of turbulent non-premixed ammonia/air and methane/air swirl flames through a rich-lean combustor under various wall thermal boundary conditions at high pressure, Combust. Flame 210 (2019) 247–261.
[13] S Kondo, K Takizawa, A Takahashi, K Tokuhashi, A Sekiya, A study on flammability limits of fuel mixtures, J. Hazard. Mater. 155 (3) (2008) 440–448.
[14] S Kondo, K Takizawa, A Takahashi, K Tokuhashi, On the temperature dependence of flammability limits of gases, J. Hazard. Mater. 187 (1–3) (2011) 585–590.
[15] A Valera-Medina, D G Pugh, P Marsh, G Bulat, P Bowen, Preliminary study on lean premixed combustion of ammonia-hydrogen for swirling gas turbine combustors, Int. J. Hydrogen Energy 42 (38) (2017) 24495–24503.
[16] M Guteša Božo, M O Vigueras-Zuniga, M Buffi, T Seljak, A Valera-Medina, Fuel rich ammonia-hydrogen injection for humidified gas turbines, Appl. Energy 251 (2019), doi:10.1016/j.apenergy.2019.113334.
[17] A Valera-Medina, R Marsh, J Runyon, D Pugh, P Beasley, T Hughes, P Bowen, Ammonia-methane combustion in tangential swirl burners for gas turbine power generation, Appl. Energy 185 (2017) 1362–1371.

[18] H Xiao, M Howard, A Valera-Medina, S Dooley, P J Bowen, Study on reduced chemical mechanisms of ammonia/methane combustion under gas turbine conditions, Energy Fuels 30 (10) (2016) 8701–8710.
[19] N A Hussein, A Valera-Medina, A S Alsaegh, Ammonia-hydrogen combustion in a swirl burner with reduction of NOx emissions, Energy Procedia 158 (2019) 2305–2310.
[20] H Xiao, A Valera-Medina, P J Bowen, Study on premixed combustion characteristics of co-firing ammonia/methane fuels, Energy 140 (2017) 125–135.
[21] K D K A Somarathne, S Colson, A Hayakawa, H Kobayashi, Modelling of ammonia/air non-premixed turbulent swirling flames in a gas turbine-like combustor at various pressures, Combust. Theory Modell. 22 (5) (2018) 973–997.
[22] D Pugh, P Bowen, A Valera-Medina, A Giles, J Runyon, R Marsh, Influence of steam addition and elevated ambient conditions on NO_x reduction in a staged premixed swirling NH_3/H_2 flame, Proc. Combust. Inst. 37 (4) (2019) 5401–5409.
[23] Q G Peng, W M Yang, E JQ, H P Xu, Z W Li, K L Tay, G Zeng, W B Yu, Investigation on premixed H_2/C_3H_8/air combustion in porous medium combustor for the micro thermophotovoltaic application, Appl. Energy 260 (2020), doi:10.1016/j.apenergy.2019.114352.
[24] W M Yang, S K Chou, K J Chua, H An, K Karthikeyan, X Zhao, An advanced micro modular combustor-radiator with heat recuperation for micro-TPV system application, Appl. Energy 97 (2012) 749–753.
[25] A W Fan, Y Xiang, W Yang, L H Li, Enhancement of hydrogen combustion efficiency by helium dilution in a micro-combustor with wall cavities, Chem. Eng. Process: Process Intensif. 130 (2018) 201–207.
[26] Q H Huang, A K Tang, T Cai, D Zhao, C Zhou, Entropy generation analysis of combustion process adopting blended propane/hydrogen fuels in micro-combustor, Chem. Eng. Process: Process Intensif. 143 (2019), doi:10.1016/j.cep.2019.107601.
[27] H Nakamura, S Hasegawa, T Tezuka, Kinetic modeling of ammonia/air weak flames in a micro flow reactor with a controlled temperature profile, Combust. Flame 185 (2017) 16–27.
[28] H Nakamura, S Hasegawa, Combustion and ignition characteristics of ammonia/air mixtures in a micro flow reactor with a controlled temperature profile, Proc. Combust. Inst. 36 (3) (2017) 4217–4226.
[29] E C Okafor, K D Somarathne, A Kunkuma, A Hayakawa, T Kudo, O Kurata, N Iki, H Kobayashi, Towards the development of an efficient low-NOx ammonia combustor for a micro gas turbine, Proc. Combust. Inst. 37 (4) (2019) 4597–4606.
[30] E C Okafor, K D K A Somarathne, R Ratthanan, A Hayakawa, T Kudo, O Kurata, N Iki, T Tsujimura, H Furutani, H Kobayashi, Control of NOx and other emissions in micro gas turbine combustors fuelled with mixtures of methane and ammonia, Combust. Flame 211 (2020) 406–416.
[31] Y G Ju, K Maruta, Microscale combustion: technology development and fundamental research, Prog. Energy Combust. Sci. 37 (6) (2011) 669–715.
[32] N S Kaisare, D G Vlachos, A review on microcombustion: fundamentals, devices and applications, Prog. Energy Combust. Sci. 38 (3) (2012) 321–359.
[33] D Y Jiang, W M Yang, K J Chua, J Y Ouyang, Thermal performance of micro-combustors with baffles for thermophotovoltaic system, Appl. Therm. Eng. 61 (2) (2013) 670–677.
[34] A K Tang, T Cai, Q H Huang, J Deng, J F Pan, Numerical study on energy conversion performance of micro-thermophotovoltaic system adopting a heat recirculation micro-combustor, Fuel Process. Technol. 180 (2018) 23–31.
[35] M C Drake, R J Blint, Thermal NOx in stretched laminar opposed-flow diffusion flames with $CO/H_2/N_2$ fuel, Combust. Flame 76 (1989) 151–167.
[36] C H Kuo, P D Ronney, Numerical modeling of non-adiabatic heat-recirculating combustors, Proc. Combust. Inst. 31 (2) (2007) 3277–3284.
[37] ANSYS Fluent User's Guide, Release 18.1, ANSYS, Inc., 2017 April.
[38] W Zuo, E JQ, H L Liu, Q G Peng, X H Zhao, Z Q Zhang, Numerical investigations on an improved micro-cylindrical combustor with rectangular rib for enhancing heat transfer, Appl. Energy 184 (2016) 77–87.
[39] W M Yang, K J Chua, J F Pan, D Y Jiang, H An, Development of micro-thermophotovoltaic power generator with heat recuperation, Energy Convers. Manage. 78 (2014) 81–87.
[40] L H Li, S X Wang, L Zhao, A Fan, A numerical investigation on non-premixed catalytic combustion of $CH_4/(O_2+N_2)$ in a planar micro-combustor, Fuel 255 (2019), doi:10.1016/j.fuel.2019.115823.
[41] H Bongers, L P H De Goey, The effect of simplified transport modeling on the burning velocity of laminar premixed flames, Combust. Sci. Technol. 175 (10) (2003) 1915–1928.
[42] Q G Peng, E JQ, J W Chen, W Zuo, X H Zhao, Z Q Zhang, Investigation on the effects of wall thickness and porous media on the thermal performance of a non-premixed hydrogen fueled cylindrical micro combustor, Energy Convers. Manage. 155 (2018) 276–286.
[43] A W Fan, L H Li, W Yang, Z L Yuan, Comparison of combustion efficiency between micro combustors with single- and double-layered walls: a numerical study, Chem Eng Process: Process Intensif 137 (2019) 39–47.
[44] J L Wan, A W Fan, Y Liu, H Yao, W Liu, X L Gou, D Q Zhao, Experimental investigation and numerical analysis on flame stabilization of CH4/air mixture in a mesoscale channel with wall cavities, Combust. Flame 162 (4) (2015) 1035–1045.
[45] A K Tang, Y Xu, J F Pan, W M Yang, D Y Jiang, Q B Lu, Combustion characteristics and performance evaluation of premixed methane/air with hydrogen addition in a micro-planar combustor, Chem. Eng. Sci. 131 (2015) 235–242.
[46] W Zuo, E JQ, W Y Hu, Y Jin, D D Han, Numerical investigations on combustion characteristics of H_2/air premixed combustion in a micro elliptical tube combustor, Energy 126 (2017) 1–12.
[47] E JQ, Q G Peng, X H Zhao, W Zuo, Z Q Zhang, M Pham, Numerical investigation on the combustion characteristics of non-premixed hydrogen-air in a novel micro-combustor, Appl. Therm. Eng. 110 (2017) 665–677.